Editors' Suggestion | Featured in Physics

High-Statistics Measurement of the Cosmic-Ray Electron Spectrum with H.E.S.S.

F. Aharonian,[1,2,3] F. Ait Benkhali,[4] J. Aschersleben,[5] H. Ashkar,[6] M. Backes,[7,8] V. Barbosa Martins,[9] R. Batzofin,[10] Y. Becherini,[11,12] D. Berge,[9,13] K. Bernlöhr,[2] B. Bi,[14] M. Böttcher,[8] C. Boisson,[15] J. Bolmont,[16] M. de Bony de Lavergne,[17] J. Borowska,[13] M. Bouyahiaoui,[2] R. Brose,[1] A. Brown,[18] F. Brun,[17] B. Bruno,[19] T. Bulik,[20] C. Burger-Scheidlin,[1] T. Bylund,[17] S. Casanova,[21] J. Celic,[19] M. Cerruti,[11] T. Chand,[8] S. Chandra,[8] A. Chen,[22] J. Chibueze,[8] O. Chibueze,[8] T. Collins,[10] G. Cotter,[18] J. Damascene Mbarubucyeye,[9] J. Devin,[23] J. Djuvsland,[2] A. Dmytriiev,[8] K. Egberts,[10,*] S. Einecke,[24] J.-P. Ernenwein,[25] S. Fegan,[6] K. Feijen,[11] G. Fontaine,[6] S. Funk,[19] S. Gabici,[11] Y. A. Gallant,[23] J. F. Glicenstein,[17] J. Glombitza,[19] G. Grolleron,[16] B. Heß,[14] W. Hofmann,[2,*] T. L. Holch,[9] M. Holler,[26] D. Horns,[27] Zhiqiu Huang,[2] M. Jamrozy,[28] F. Jankowsky,[4] V. Joshi,[19] I. Jung-Richardt,[19] E. Kasai,[7] K. Katarzyński,[29] D. Kerszberg,[16] R. Khatoon,[8] B. Khélifi,[11] W. Kluźniak,[30] Nu. Komin,[22] K. Kosack,[17] D. Kostunin,[9] A. Kundu,[8] R. G. Lang,[19] S. Le Stum,[25] F. Leitl,[19] A. Lemière,[11] M. Lemoine-Goumard,[31] J.-P. Lenain,[16] F. Leuschner,[14] A. Luashvili,[15] J. Mackey,[1] D. Malyshev,[14] D. Malyshev,[19] V. Marandon,[17] P. Marinos,[24] G. Martí-Devesa,[26] R. Marx,[4] M. Meyer,[32] A. Mitchell,[19] R. Moderski,[30] M. O. Moghadam,[10] L. Mohrmann,[2] A. Montanari,[4] E. Moulin,[17] M. de Naurois,[6,*] J. Niemiec,[21] S. Ohm,[9] L. Olivera-Nieto,[2] E. de Ona Wilhelmi,[9] M. Ostrowski,[28] S. Panny,[26] M. Panter,[2] D. Parsons,[13] U. Pensec,[16] G. Peron,[11] G. Pühlhofer,[14] M. Punch,[11] A. Quirrenbach,[4] S. Ravikularaman,[11,2] M. Regeard,[11] A. Reimer,[26] O. Reimer,[26] I. Reis,[17] H. Ren,[2] B. Reville,[2] F. Rieger,[2] G. Rowell,[24] B. Rudak,[30] E. Ruiz-Velasco,[2] V. Sahakian,[36] H. Salzmann,[14] A. Santangelo,[14] M. Sasaki,[19] J. Schäfer,[19] F. Schüssler,[17] H. M. Schutte,[8] J. N. S. Shapopi,[7] A. Sharma,[11] H. Sol,[15] S. Spencer,[19] Ł. Stawarz,[28] S. Steinmassl,[2] C. Steppa,[10] H. Suzuki,[33] T. Takahashi,[34] T. Tanaka,[33] A. M. Taylor,[9] R. Terrier,[11] M. Tsirou,[9] C. van Eldik,[19] M. Vecchi,[5] C. Venter,[8] J. Vink,[35] T. Wach,[19] S. J. Wagner,[4] A. Wierzcholska,[21] M. Zacharias,[4,8] A. A. Zdziarski,[30] A. Zech,[15] and N. Żywucka[8]

(H.E.S.S. Collaboration)

[1]*Dublin Institute for Advanced Studies, 31 Fitzwilliam Place, Dublin 2, Ireland*
[2]*Max-Planck-Institut für Kernphysik, P.O. Box 103980, D 69029 Heidelberg, Germany*
[3]*Yerevan State University, 1 Alek Manukyan Street, Yerevan 0025, Armenia*
[4]*Landessternwarte, Universität Heidelberg, Königstuhl, D 69117 Heidelberg, Germany*
[5]*Kapteyn Astronomical Institute, University of Groningen, Landleven 12, 9747 AD Groningen, The Netherlands*
[6]*Laboratoire Leprince-Ringuet, École Polytechnique, CNRS, Institut Polytechnique de Paris, F-91128 Palaiseau, France*
[7]*University of Namibia, Department of Physics, Private Bag 13301, Windhoek 10005, Namibia*
[8]*Centre for Space Research, North-West University, Potchefstroom 2520, South Africa*
[9]*Deutsches Elektronen-Synchrotron DESY, Platanenallee 6, 15738 Zeuthen, Germany*
[10]*Institut für Physik und Astronomie, Universität Potsdam, Karl-Liebknecht-Strasse 24/25, D 14476 Potsdam, Germany*
[11]*Université de Paris, CNRS, Astroparticule et Cosmologie, F-75013 Paris, France*
[12]*Department of Physics and Electrical Engineering, Linnaeus University, 351 95 Växjö, Sweden*
[13]*Institut für Physik, Humboldt-Universität zu Berlin, Newtonstrasse 15, D 12489 Berlin, Germany*
[14]*Institut für Astronomie und Astrophysik, Universität Tübingen, Sand 1, D 72076 Tübingen, Germany*
[15]*Laboratoire Univers et Théories, Observatoire de Paris, Université PSL, CNRS, Université Paris Cité, 5 place Jules Janssen, 92190 Meudon, France*
[16]*Sorbonne Université, CNRS/IN2P3, Laboratoire de Physique Nucléaire et de Hautes Energies, LPNHE, 4 place Jussieu, 75005 Paris, France*
[17]*IRFU, CEA, Université Paris-Saclay, F-91191 Gif-sur-Yvette, France*
[18]*Department of Physics, University of Oxford, Denys Wilkinson Building, Keble Road, Oxford OX1 3RH, United Kingdom*
[19]*Friedrich-Alexander-Universität Erlangen-Nürnberg, Erlangen Centre for Astroparticle Physics, Nikolaus-Fiebiger-Strasse 2, 91058 Erlangen, Germany*
[20]*Astronomical Observatory, The University of Warsaw, Aleje Ujazdowskie 4, 00-478 Warsaw, Poland*
[21]*Instytut Fizyki Jądrowej PAN, ulica Radzikowskiego 152, 31-342 Kraków, Poland*
[22]*School of Physics, University of the Witwatersrand, 1 Jan Smuts Avenue, Braamfontein, Johannesburg 2050, South Africa*
[23]*Laboratoire Univers et Particules de Montpellier, Université Montpellier, CNRS/IN2P3, CC 72, Place Eugène Bataillon, F-34095 Montpellier Cedex 5, France*
[24]*School of Physical Sciences, University of Adelaide, Adelaide, South Australia 5005, Australia*
[25]*Aix Marseille Université, CNRS/IN2P3, CPPM, Marseille, France*
[26]*Universität Innsbruck, Institut für Astro- und Teilchenphysik, Technikerstraße 25, 6020 Innsbruck, Austria*

[27]Institut für Experimentalphysik, Universität Hamburg, Luruper Chaussee 149, D 22761 Hamburg, Germany
[28]Obserwatorium Astronomiczne, Uniwersytet Jagielloński, ulica Orla 171, 30-244 Kraków, Poland
[29]Institute of Astronomy, Faculty of Physics, Astronomy and Informatics, Nicolaus Copernicus University, Grudziadzka 5, 87-100 Torun, Poland
[30]Nicolaus Copernicus Astronomical Center, Polish Academy of Sciences, ulica Bartycka 18, 00-716 Warsaw, Poland
[31]Université Bordeaux, CNRS, LP2I Bordeaux, UMR 5797, F-33170 Gradignan, France
[32]University of Southern Denmark, 5230 Odense, Denmark
[33]Department of Physics, Konan University, 8-9-1 Okamoto, Higashinada, Kobe, Hyogo 658-8501, Japan
[34]Kavli Institute for the Physics and Mathematics of the Universe (WPI), The University of Tokyo Institutes for Advanced Study (UTIAS), The University of Tokyo, 5-1-5 Kashiwa-no-Ha, Kashiwa, Chiba 277-8583, Japan
[35]GRAPPA, Anton Pannekoek Institute for Astronomy, University of Amsterdam, Science Park 904, 1098 XH Amsterdam, The Netherlands
[36]Yerevan Physics Institute, 2 Alikhanian Brothers Street, 0036 Yerevan, Armenia

(Received 15 June 2024; accepted 24 September 2024; published 25 November 2024)

Owing to their rapid cooling rate and hence loss-limited propagation distance, cosmic-ray electrons and positrons (CRe) at very high energies probe local cosmic-ray accelerators and provide constraints on exotic production mechanisms such as annihilation of dark matter particles. We present a high-statistics measurement of the spectrum of CRe candidate events from 0.3 to 40 TeV with the High Energy Stereoscopic System, covering 2 orders of magnitude in energy and reaching a proton rejection power of better than 10^4. The measured spectrum is well described by a broken power law, with a break around 1 TeV, where the spectral index increases from $\Gamma_1 = 3.25 \pm 0.02(\text{stat}) \pm 0.2(\text{sys})$ to $\Gamma_2 = 4.49 \pm 0.04(\text{stat}) \pm 0.2(\text{sys})$. Apart from the break, the spectrum is featureless. The absence of distinct signatures at multi-TeV energies imposes constraints on the presence of nearby CRe accelerators and the local CRe propagation mechanisms.

DOI: 10.1103/PhysRevLett.133.221001

Introduction—Cosmic-ray electrons and positrons (CRe) at very high energies ($E \gtrsim 100$ GeV) undergo fast radiation losses while propagating in the Galaxy. Both inverse-Compton scattering and synchrotron radiation losses limit their cooling times and therefore propagation distance to typically kiloparsec scales or below [1,2] in diffusion-dominated Galactic cosmic-ray transport [3]. Therefore, local CRe either indicate the existence of one (or several) primary CRe sources in the local vicinity [4,5] or are the result of cosmic-ray nuclei interacting with interstellar gas producing secondary CRe [6], which would suggest a more distributed origin of CRe. In particular, nearby pulsars and their environments as well as supernova remnants have been suggested as CRe sources [7–10]. However, no unambiguous imprint of such local CRe sources has been revealed in the spectrum, nor inferred through anisotropy [11–14] of the CRe observed at Earth. The measurements of the positron fraction rising with energy [15,16] triggered interest in more exotic scenarios, such as the imprint of dark matter annihilation, although conventional scenarios with pulsars as CRe sources seem to be favored [17–19]. The high-energy end of the CRe spectrum has been made accessible by indirect, ground-based measurement techniques. High Energy Stereoscopic System (H.E.S.S.) measurements up to ∼4 TeV [20,21] revealed the existence of a break in the CRe spectrum at around 1 TeV, confirmed later by MAGIC and VERITAS [22,23]. Direct measurements by the *Fermi* Large Area Telescope (*Fermi*-LAT) and AMS-02 reached the onset of the break in the electron spectrum [24,25], allowed for discrimination between electrons and positrons [26], and ultimately extended the energy range of direct measurements [27]. Further extension to 4.6 and 7.5 TeV, respectively, and a first confirmation of the break by direct measurements was obtained by DAMPE [28] and CALET [29].

Using the vast statistics provided by 12 years of data, advanced particle discrimination schemes, and improved instrument response functions, we now constrain the CRe measurement to an unequaled energy of 40 TeV and resolve the spectral break with high statistics.

The dataset—H.E.S.S. is an array of imaging atmospheric Cherenkov telescopes (IACTs) situated in Namibia, with four 12 m diameter telescopes (CT1–4), operational since 2003, and one large-size telescope with a mirror diameter of 28 m in the center of the array (CT5), inaugurated in 2012. H.E.S.S. has proven its capability to measure CRe already in 2008 [20,21], becoming the first ground-based instrument to do so. Since leptonic charge separation cannot be achieved with H.E.S.S., measurements of the sum of electrons and positrons are performed, and the term CRe is used for the sum of both hereafter.

The cameras of the CT1–4 telescopes were upgraded in 2017 with new electronics. The analysis presented here uses all data taken with CT1–4 before the camera upgrade, spanning a period of almost 12 years of H.E.S.S. observations, from December 2003 to June 2015.

*Contact author: contact.hess@hess-experiment.eu

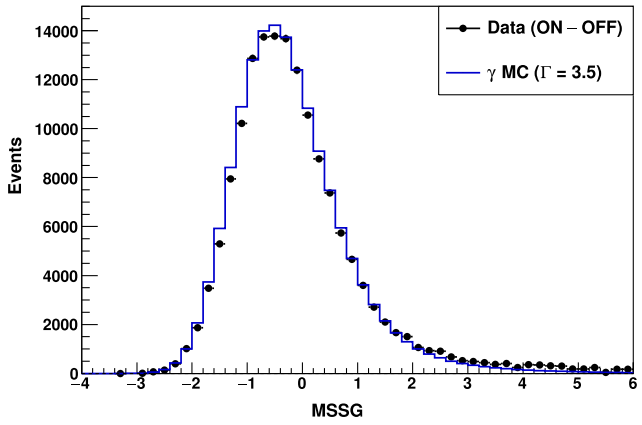

FIG. 1. The distribution of the main classifier, the MSSG, for γ rays from PKS 2155-304 in H.E.S.S. data after background subtraction (black), compared to γ-ray simulations generated with a spectral index $\Gamma = 3.5$ (blue).

Strict quality criteria have been applied to guarantee the best possible data quality. In addition to standard quality cuts [30], only observations with all four CT1–4 telescopes operational and with zenith angles smaller than 45° were used. The atmospheric transparency to Cherenkov radiation, as inferred from the trigger rate [31], is also used in the selection: only data with relative transparency larger than 60% are used.

Under the assumption of isotropy, all observations can be used for a measurement of CRe. However, since discrimination between electron and γ-ray-induced air showers is challenging, the Galactic plane with its very extended γ-ray sources [32] and diffuse γ-ray emission [33] is excluded within $\pm 15°$ of latitude. Runs with pointing positions within 5° from the Small and Large Magellanic Clouds are also excluded. This selection results in a total of 6830 observation runs corresponding to ∼2728 h of data. Only events that are reconstructed to originate from within the central 4° of the 5° diameter field of view are retained. Events within 0.25° radius from known very-high-energy γ-ray sources are also rejected (the H.E.S.S. point spread function for these data is typically 0.06°).

Potential remaining contaminations are the high-latitude Galactic diffuse emission and the diffuse extragalactic γ-ray background, which has a flux well below the CRe flux and shows an exponential cutoff at 250 GeV [34].

Monte Carlo simulations—Monte Carlo (MC) simulations of IACTs are used at the reconstruction level to correct data for instrumental or environmental effects, at the analysis level for validation, and at the spectral reconstruction level, where precise instrument response functions are needed.

Standard IACT analyses use interpolations between pregenerated MC datasets generated on a fixed grid of the parameter space. Here a more precise approach is used: In the runwise simulation scheme [35], every run is simulated with the actual source trajectory and instrument parameters of that run. This improves the agreement between data and simulations [35] and provides more accurate response functions.

For each run of the dataset, a large number of electron-induced showers (typically on the order of 200 000) are simulated with a hard spectrum ($\Gamma = 1.3$), ensuring sufficient statistics at high energies and reliable response functions up to more than 80 TeV. This MC dataset is used at different levels of the analysis to check the quality and stability of the results (see Supplemental Material [30]).

Shower reconstruction and primary particle identification—For the event reconstruction, an advanced reconstruction technique (Model + +) based on comparison of the camera images with a semianalytical model of the air showers is applied [36]. The shower image goodness of fit allows selection of relatively clean samples of γ-ray or CRe candidate events. The goodness of fit of each image is rescaled by computing its difference to its mean as derived from γ-ray simulations and dividing the result by its rms. This allows us to combine the results of each telescope in a single variable, the mean scaled shower goodness (MSSG). Given the similarity between the CRe and γ-ray shower development, this goodness-of-fit MSSG has a rather similar distribution for both primary γ rays and CRe. For the analysis of γ-ray sources, the cut value on MSSG is chosen as a compromise between statistics of γ-ray candidates and background level, given that the remaining background can be reliably determined from off-source regions, and subtracted. For the investigation of the diffuse CRe flux, the

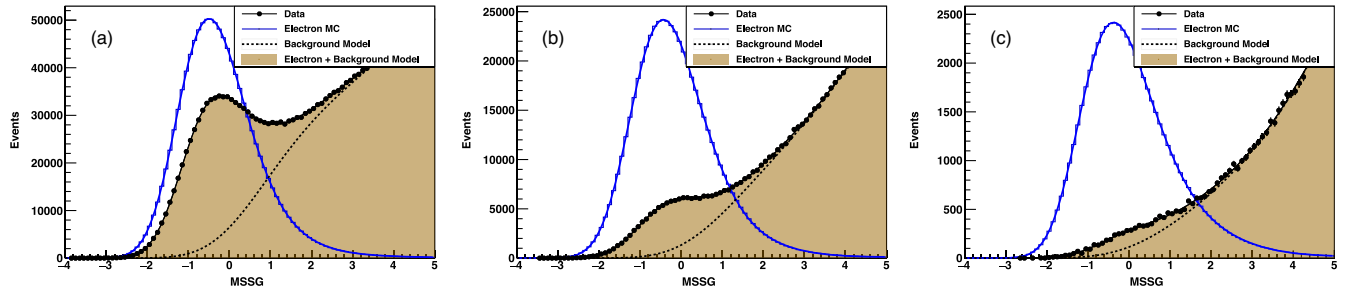

FIG. 2. The MSSG distribution for H.E.S.S. data (black data points) in three energy bands: (a) 0.3–1 TeV, (b) 1–3 TeV, and (c) > 3 TeV. The data are fitted with a parametrization of simulated electrons (blue, arb. norm.) and a parametrization of the hadronic cosmic rays (black dashed line). The combined model of electrons and hadronic background is shown as the solid black line and ocher area.

MSSG is calculated assuming the electron hypothesis, and a hard cut of MSSG < -0.6 is used, together with additional selections cuts (see Supplemental Material [30]). This drastically reduces the background of cosmic-ray protons and nuclei (CRn) among the CRe candidate events, at the expense of signal statistics, resulting in a proton rejection of better than 10^4 at a few TeV.

This technique crucially relies on the ability of the simulations to accurately reproduce the MSSG distribution for electromagnetic air showers. This was validated using the MSSG distribution for γ rays from the blazar PKS 2155-304 (using a dataset of 755 runs), after subtracting the cosmic-ray background. The distribution is compared to γ-ray simulations obtained within the runwise scheme. Identical cuts were used for selection of runs, images, and events as for the CRe sample. As illustrated in Fig. 1, the measured distribution is indeed well reproduced by simulations, see also Supplemental Material [30].

In Fig. 2 the measured distribution in MSSG is shown, in three energy ranges (ocher histograms), in comparison to electron runwise simulations (blue curves). The data distributions exhibit a clear peak consistent with the electron simulations, on top of a much broader distribution that corresponds to CRn. The data are modeled as a sum of the simulated MSSG distribution of electrons and an analytical parametrization (dotted line) to account for the CRn background. The resulting distribution—shown as a solid black line—is in good agreement with the data, although it should be noted that there is some freedom in the choice of the analytical parametrization representing the hadronic background.

The analysis presented here deliberately avoids using distributions from simulated CRn and does not attempt to subtract the CRn remaining after the CRe selection cuts. CRn simulations have considerably larger uncertainties than those of electromagnetic cascades, due to the model dependence in the simulation of hadronic interactions. Moreover, the fraction of hadronic showers triggering the instrument and passing the selection cuts is much lower than for electromagnetic showers, making the production of a CRn Monte Carlo dataset excessive in terms of computing time.

From Fig. 2, an estimate of the remaining CRn contamination as a function of the MSSG cut can be obtained. Below MSSG $\simeq -1$, where very little CRn contamination is expected, the measured MSSG distribution is in excellent agreement with the predictions for electrons. For MSSG $\gtrsim -1$, an increasing excess over the electron simulations is seen, which is attributed to CRn. The applied cut of MSSG ≤ -0.6 results in a CRn contamination in the CRe dataset of less than 25% for the energy range of 0.1–1 TeV and less than 30% for 1–3 TeV. Beyond 3 TeV a dominant background contribution cannot be excluded [30].

Spectrum of electron + positron *candidate events*—This analysis resulted in the selection of 265 574 electronlike events from 0.3 to 40 TeV. The energy spectrum for these events is derived using a forward-folding procedure assuming that all selected events are electrons and using instrument response functions computed from electron simulations described above. The red data points in Fig. 3 show the resulting spectrum of these CRe candidate events along with previous CRe measurements. Numerical values are provided in Supplemental Material [30].

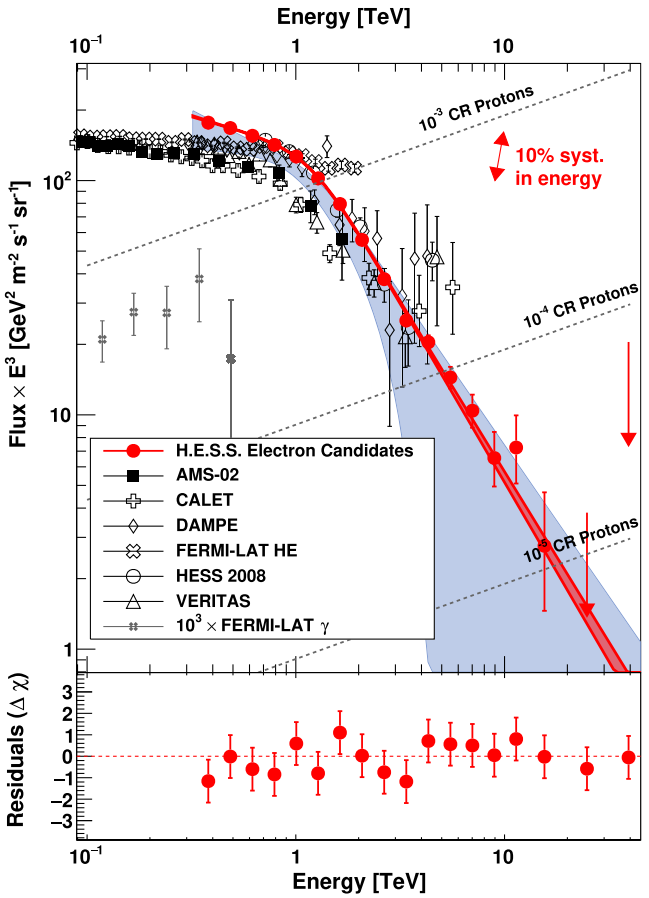

FIG. 3. Filled red circle data points: spectrum of CRe candidate events measured by H.E.S.S. The dataset still contains a residual background from CRn and therefore places an upper limit on the true CRe flux. The dark red band indicates the broken-power-law fit to the data [Eq. (1)], with the width of the band corresponding to statistical errors. The light blue band denotes the estimated range of the true CRe flux, considering the CRn contamination as well as the statistical errors and systematic errors. Separately shown is the systematic error on the global energy scale, which also impacts the normalization of $E^3F(E)$, as visualized by the red arrow. Included are CRe measurements by AMS-02 [25], *Fermi*-LAT [27], CALET [29], DAMPE [28], VERITAS [23], and previous H.E.S.S. measurements [20,21]. Also shown is the CR proton flux based on AMS-02 [37] and DAMPE [38] data (scaled down by $10^{-3} - 10^{-5}$) and the *Fermi*-LAT diffuse extragalactic γ-ray flux [34] (scaled up by 10^3). The bottom panel shows the residuals expressed in $\Delta\chi = (\phi_i - \phi(E))/\sigma_i$ where ϕ_i and σ_i are, respectively, the flux measured in bin i and its statistical uncertainty, and $\phi(E)$ is the expected flux from Eq. (1).

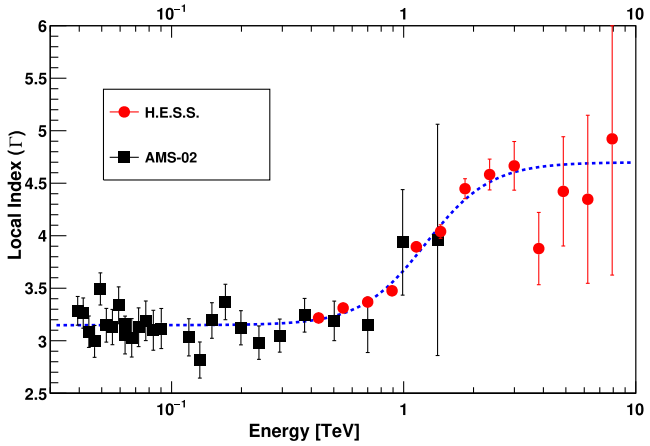

FIG. 4. Local spectral index, calculated from adjacent data points as $\Gamma(E) = \Delta \log \phi / \Delta \log E$, for the high-statistics H.E.S.S. and AMS-02 [25] spectra. H.E.S.S. data are described by a sigmoid function in $\log E$, shown as a blue dashed line.

The spectrum of CRe candidate events is consistent with an otherwise featureless broken power law with a break around 1 TeV,

$$F(E) = F_0 \left(\frac{E}{1\ \mathrm{TeV}}\right)^{-\Gamma_1} \left[1 + \left(\frac{E}{E_b}\right)^{\frac{1}{\alpha}}\right]^{-(\Gamma_2-\Gamma_1)\alpha} \quad (1)$$

with $F_0 = (126.1 \pm 0.5_{\mathrm{stat}} \pm 13_{\mathrm{sys}})\ \mathrm{GeV}^2\,\mathrm{m}^{-2}\,\mathrm{sr}^{-1}\,\mathrm{s}^{-1}$ as flux normalization; $\Gamma_1 = 3.25 \pm 0.02_{\mathrm{stat}} \pm 0.2_{\mathrm{sys}}$ as the low-energy index of the power law; $\Gamma_2 = 4.49 \pm 0.04_{\mathrm{stat}} \pm 0.2_{\mathrm{sys}}$ as the high-energy index of the power law; $E_b = (1.17 \pm 0.04_{\mathrm{stat}} \pm 0.12_{\mathrm{sys}})$ TeV as the break energy; and $\alpha = 0.21 \pm 0.02_{\mathrm{stat}}\,{}^{+0.10_{\mathrm{sys}}}_{-0.06_{\mathrm{sys}}}$ as the sharpness of the break.

The dark red band in Fig. 3 indicates the best fit to the data, with the width of the band corresponding to the statistical errors of the data.

Systematic errors of the parameters described in Eq. (1) are derived by varying analysis cuts as well as accounting for the variation of the observed flux with zenith angle, with atmospheric conditions and with time, i.e., aging of the instrument, see Supplemental Material [30]. An additional error on F_0 and E_b arises from a 10% uncertainty on the global energy scale, which translates into a 21% uncertainty in the energy-weighted F_0, as indicated by the double-headed red arrows in Fig. 3.

In the energy range of overlap, the measured flux $E^3F(E)$ of CRe candidate events is overall about 30% higher compared to other measurements. Taking into account systematic uncertainties and the estimates of a typical 15% hadronic contamination at energies below 3 TeV [30], the estimated range of the true CRe spectrum (visualized as blue-shaded area in Fig. 3) is compatible to other measurements.

The high statistics of the H.E.S.S. data allow us to determine a local spectral index of CRe candidate events, calculated as $\Gamma(E) = \Delta \log \phi / \Delta \log E$ for data points adjacent in E (Fig. 4). The calculation uses the resolution-unfolded spectra; given the energy resolution of better than 10% (see Fig. 5 of [30]), resolution corrections are modest. Also included in Fig. 4 is the local spectral index calculated for AMS-02 data [25]. The variation of the spectral index across the break is well described by a sigmoid function in $\log E$.

Discussion and conclusion—The analysis of an extended dataset from H.E.S.S. led to the identification of a vastly increased number of CRe-like events compared to the previous H.E.S.S. measurement [20], extending to energies of 40 TeV. The spectrum of CRe candidate events is well described by a broken power law. The break at 1.17 TeV is relatively sharp; the index change—consistent with a $\Delta\Gamma = 1$ cooling break—occurs over a factor 3 in energy.

This sample of CRe candidate events contains a contamination of CRn. For energies up to ∼3 TeV—well above the break—the contamination can be estimated from the shape of the MSSG distribution (Fig. 2) and is smaller than 30%; in this domain the measured spectral shape can be taken as representative for the true CRe. At higher energies, the contamination increases in accordance with the much steeper CRe spectrum compared to the CRn spectrum with its spectral index of about 2.7. With increasing energy it is therefore increasingly difficult to limit the contamination (see Fig. 3). The measured spectrum at the highest energies should be considered an upper limit for the true CRe flux; the range of the true CRe flux is indicated by the light blue area in Fig. 3.

Beyond CRe, γ rays from the diffuse γ-ray background are also likely to pass the event selection cuts. However, given the measured isotropic diffuse flux [34], this contamination is plausibly negligible across the energy range covered (see Fig. 3). Taking the well-measured *Fermi*-LAT results as indicative for the TeV range [39], also the flux of high-latitude Galactic diffuse emission is still significantly lower than the measured CRe spectrum. This is supported by the lack of variation of the spectrum normalization as function of Galactic latitude (see [30], Fig. 18).

For the sub-TeV CRe flux, there is a ∼30% significant difference between AMS-02 and CALET data on the one hand and Fermi-LAT and DAMPE on the other hand. The systematic errors of the H.E.S.S. flux normalization do not give preference to one or the other group of data. The measured low-energy spectral index of $\Gamma_1 = 3.25$ is slightly larger than the indices in the range of ∼3.1 (*Fermi*-LAT, DAMPE) to ∼3.2 (AMS-02) measured by other experiments, but fully compatible within statistical and systematic errors. The measured break energy of $E_b = 1.17$ TeV is, within systematic errors, marginally compatible with the DAMPE value of 0.91 TeV, but is significantly larger than the break of 0.71 TeV quoted by VERITAS. Also the *Fermi*-LAT lower limit (95% CL) for the break energy of 1.8 TeV is not compatible with the clear and

highly significant spectral break observed with H.E.S.S. and other experiments.

At high energy, the H.E.S.S. spectrum of CRe candidate events extends well beyond the direct measurements presented recently [28,29] and other indirect measurements. The high-energy index of $\Gamma_2 = 4.49$ obtained with H.E.S.S. for the spectrum of CRe candidates is larger than the values of 3.92 of DAMPE and 4.1 of VERITAS. Given that the CRe candidates include a CRn background whose relative importance is increasing with energy, the measured value should be interpreted as a lower limit for the true CRe high-energy index, and a high-energy cutoff is not excluded.

The H.E.S.S. data do not confirm the existence of a 1.4 TeV peak in the spectrum, which has been associated with a dark matter signal [40], nor the rise observed by various experiments in their last energy points around 5 TeV.

The detection of a multi-TeV CRe flux and the associated spectral break probe local CRe accelerators. The rapid cooling at these energies imposes limitations on both the electrons' energy-loss time ($\sim$100 kyr) and their propagation distance (a few hundred parsecs). The H.E.S.S. results dismiss the presence of a strong close-by source causing a rise in $E^3F(E)$ at multi-TeV energies (e.g., [8]) and impose limits on local sources: In a burstlike scenario, a Vela-type source with a distance of 300 pc and an age of 11 kyr is limited to a maximum energy of $\sim 2 \times 10^{46}$ erg released in electrons (see Supplemental Material [30]).

The high statistics of the H.E.S.S. data allow us to characterize the shape of the observed spectral break. A sharp break [$\alpha = 0$ in Eq. (1)] is excluded with high confidence; the break can be characterized by an α of 0.21, implying that the index changes by about unity over a factor 3 in energy, as visible in Fig. 4. Uncertainties in the CRn background at higher energies prevent us from ruling out an exponential cutoff above a few TeV. Nevertheless, the identification of a break at about 1 TeV remains a robust finding and carries important information regarding CRe acceleration and propagation within the local Galaxy. For synthetic models with distributed ensembles of sources (e.g., [10,41,42]) and a corresponding spread of propagation times, one tends to obtain significantly smoother spectra than observed, with a smeared-out break. The observed, still relatively sharp break may therefore favor a scenario in which—at energies around one TeV—a single nearby source, with a burstlike release of electrons (e.g., [43,44]), takes over a population of CRe escaping from distributed sources (e.g., [45,46]), possibly resulting also in an observable anisotropy at these energies. The steep fall-off of the CRe candidate spectrum limits the capabilities of space-borne instruments to measure the multi-TeV CRe spectrum. The H.E.S.S. measurement can potentially be further improved using machine learning to select CRe; this, however, implies simulation of huge CRn background samples, which is computationally extremely expensive.

Acknowledgments—The support of the Namibian authorities and of the University of Namibia in facilitating the construction and operation of H. E. S. S. is gratefully acknowledged, as is the support by the German Ministry for Education and Research (BMBF), the Max Planck Society, the Helmholtz Association, the French Ministry of Higher Education, Research and Innovation, the Centre National de la Recherche Scientifique (CNRS/IN2P3 and CNRS/INSU), the Commissariat à l'énergie atomique et aux énergies alternatives (CEA), the U.K. Science and Technology Facilities Council (STFC), the Irish Research Council (IRC) and the Science Foundation Ireland (SFI), the Polish Ministry of Education and Science, Agreement No. 2021/WK/06, the South African Department of Science and Innovation and National Research Foundation, the University of Namibia, the National Commission on Research, Science and Technology of Namibia (NCRST), the Austrian Federal Ministry of Education, Science and Research and the Austrian Science Fund (FWF), the Australian Research Council (ARC), the Japan Society for the Promotion of Science, the University of Amsterdam, and the Science Committee of Armenia Grant No. 21AG-1C085. We appreciate the excellent work of the technical support staff in Berlin, Zeuthen, Heidelberg, Palaiseau, Paris, Saclay, Tübingen, and in Namibia in the construction and operation of the equipment. This work benefited from services provided by the H. E. S. S. Virtual Organisation, supported by the national resource providers of the EGI Federation.

[1] C. S. Shen, Pulsars and very high-energy cosmic-ray electrons, Astrophys. J. Lett. **162**, L181 (1970).
[2] R. Cowsik and M. A. Lee, On the sources of cosmic ray electrons, Astrophys. J. **228**, 297 (1979).
[3] R. R. Daniel and S. A. Stephens, Propagation of cosmic rays in the Galaxy, Space Sci. Rev. **17**, 45 (1975).
[4] E. Massaro, B. Sacco, and G. Manzo, The source distribution of cosmic-ray electrons, Astron. Astrophys. **90**, 140 (1980).
[5] A. M. Atoyan, F. A. Aharonian, and H. J. Völk, Electrons and positrons in the galactic cosmic rays, Phys. Rev. D **52**, 3265 (1995).
[6] I. V. Moskalenko and A. W. Strong, Production and propagation of cosmic-ray positrons and electrons, Astrophys. J. **493**, 694 (1998).
[7] F. A. Aharonian, A. M. Atoyan, and H. J. Völk, High energy electrons and positrons in cosmic rays as an indicator of the existence of a nearby cosmic tevatron, Astron. Astrophys. **294**, L41 (1995).
[8] T. Kobayashi, Y. Komori, K. Yoshida, and J. Nishimura, The most likely sources of high-energy cosmic-ray electrons in supernova remnants, Astrophys. J. **601**, 340 (2004). astro-ph/0308470.
[9] T. Delahaye, J. Lavalle, R. Lineros, F. Donato, and N. Fornengo, Galactic electrons and positrons at the Earth: New estimate of the primary and secondary fluxes, Astron. Astrophys. **524**, A51 (2010).

[10] C. Evoli, E. Amato, P. Blasi, and R. Aloisio, Galactic factories of cosmic-ray electrons and positrons, Phys. Rev. D **103**, 083010 (2021).
[11] S. Shen and C. Y. Mao, Anisotropy of high energy cosmic-ray electrons in the discrete source model, Astrophys. Lett. **9**, 169 (1971).
[12] V. S. Ptuskin and J. F. Ormes, Expected anisotropy of very high energy electrons, Int. Cosmic Ray Conf. **3**, 56 (1995).
[13] S. Abdollahi *et al.* (Fermi-LAT Collaboration), Search for cosmic-ray electron and positron anisotropies with seven years of *Fermi* Large Area Telescope Data, Phys. Rev. Lett. **118**, 091103 (2017).
[14] S. Manconi, M. D. Mauro, and F. Donato, Dipole anisotropy in cosmic electrons and positrons: Inspection on local sources, J. Cosmol. Astropart. Phys. 01 (2017) 006.
[15] O. Adriani *et al.* (PAMELA Collaboration), An anomalous positron abundance in cosmic rays with energies 1.5–100 GeV, Nature (London) **458**, 607 (2009).
[16] M. Aguilar *et al.* (AMS Collaboration), Electron and positron fluxes in primary cosmic rays measured with the Alpha Magnetic Spectrometer on the International Space Station, Phys. Rev. Lett. **113**, 121102 (2014).
[17] S. Profumo, J. Reynoso-Cordova, N. Kaaz, and M. Silverman, Lessons from HAWC pulsar wind nebulae observations: The diffusion constant is not a constant; pulsars remain the likeliest sources of the anomalous positron fraction; cosmic rays are trapped for long periods of time in pockets of inefficient diffusion, Phys. Rev. D **97**, 123008 (2018).
[18] X. Tang and T. Piran, Positron flux and γ-ray emission from Geminga pulsar and pulsar wind nebula, Mon. Not. R. Astron. Soc. **484**, 3491 (2019).
[19] M. Aguilar, L. Ali Cavasonza, B. Alpat, G. Ambrosi, L. Arruda, N. Attig, P. Azzarello, A. Bachlechner, F. Barao, A. Barrau *et al.*, Towards understanding the origin of cosmic-ray electrons, Phys. Rev. Lett. **122**, 101101 (2019).
[20] F. Aharonian *et al.* (H.E.S.S. Collaboration), The energy spectrum of cosmic-ray electrons at TeV energies, Phys. Rev. Lett. **101**, 261104 (2008).
[21] F. Aharonian *et al.* (H.E.S.S. Collaboration), Probing the ATIC peak in the cosmic-ray electron spectrum with H.E.S.S., Astron. Astrophys. **508**, 561 (2009).
[22] D. Borla Tridon, Measurement of the cosmic electron spectrum with the MAGIC telescopes, Int. Cosmic Ray Conf. **6**, 47 (2011).
[23] A. Archer *et al.* (VERITAS Collaboration), Measurement of cosmic-ray electrons at TeV energies by VERITAS, Phys. Rev. D **98**, 062004 (2018).
[24] M. Ackermann *et al.* (Fermi-LAT Collaboration), Fermi LAT observations of cosmic-ray electrons from 7 GeV to 1 TeV, Phys. Rev. D **82**, 092004 (2010).
[25] M. Aguilar *et al.*, The Alpha Magnetic Spectrometer (AMS) on the international space station: Part II—results from the first seven years, Phys. Rep. **894**, 1 (2021).
[26] M. Ackermann *et al.* (Fermi-LAT Collaboration), Measurement of separate cosmic-ray electron and positron spectra with the *Fermi* Large Area Telescope, Phys. Rev. Lett. **108**, 011103 (2012).
[27] S. Abdollahi *et al.* (Fermi-LAT Collaboration), Cosmic-ray electron-positron spectrum from 7 GeV to 2 TeV with the *Fermi* Large Area Telescope, Phys. Rev. D **95**, 082007 (2017).
[28] G. Ambrosi *et al.* (DAMPE Collaboration), Direct detection of a break in the teraelectronvolt cosmic-ray spectrum of electrons and positrons, Nature (London) **552**, 63 (2017).
[29] O. Adriani *et al.* (CALET Collaboration), Direct measurement of the spectral structure of cosmic-ray electrons + positrons in the TeV region with CALET on the International Space Station, Phys. Rev. Lett. **131**, 191001 (2023).
[30] See Supplemental Material at http://link.aps.org/supplemental/10.1103/PhysRevLett.133.221001 for numerical values of the data and additional information on data analysis and interpretation.
[31] J. Hahn, R. de los Reyes, K. Bernlöhr, P. Krüger, Y. T. E. Lo, P. M. Chadwick, M. K. Daniel, C. Deil, H. Gast, K. Kosack, and V. Marandon, Impact of aerosols and adverse atmospheric conditions on the data quality for spectral analysis of the H.E.S.S. telescopes, Astropart. Phys. **54**, 25 (2014).
[32] H. Abdalla *et al.* (H.E.S.S. Collaboration), The H.E.S.S. Galactic plane survey, Astron. Astrophys. **612**, A1 (2018).
[33] A. Abramowski *et al.* (H.E.S.S. Collaboration), Diffuse Galactic gamma-ray emission with H.E.S.S., Phys. Rev. D **90**, 122007 (2014).
[34] M. Ackermann *et al.* (Fermi-LAT Collaboration), The spectrum of isotropic diffuse gamma-ray emission between 100 MeV and 820 GeV, Astrophys. J. **799**, 86 (2015).
[35] M. Holler, J. P. Lenain, M. de Naurois, R. Rauth, and D. A. Sanchez, A run-wise simulation and analysis framework for imaging atmospheric Cherenkov telescope arrays, Astropart. Phys. **123**, 102491 (2020).
[36] M. de Naurois and L. Rolland, A high performance likelihood reconstruction of γ-rays for imaging atmospheric Cherenkov telescopes, Astropart. Phys. **32**, 231 (2009).
[37] J. Alcaraz *et al.* (AMS-02 Collaboration), Cosmic protons, Phys. Lett. B **490**, 27 (2000).
[38] Q. An *et al.* (DAMPE Collaboration), Measurement of the cosmic ray proton spectrum from 40 GeV to 100 TeV with the DAMPE satellite, Sci. Adv. **5**, eaax3793 (2019).
[39] M. Ackermann *et al.*, Fermi-LAT observations of the diffuse γ-ray emission: Implications for cosmic rays and the interstellar medium, Astrophys. J. **750**, 3 (2012).
[40] Q. Yuan *et al.*, Interpretations of the DAMPE electron data, arXiv:1711.10989.
[41] P. Mertsch, Stochastic cosmic ray sources and the TeV break in the all-electron spectrum, J. Cosmol. Astropart. Phys., 11 (2018) 045.
[42] K. Asano, Y. Asaoka, Y. Akaike, N. Kawanaka, K. Kohri, H. M. Motz, and T. Terasawa, Monte Carlo study of electron and positron cosmic-ray propagation with the CALET spectrum, Astrophys. J. **926**, 5 (2022).
[43] M. D. Mauro, F. Donato, N. Fornengo, R. Lineros, and A. Vittino, Interpretation of AMS-02 electrons and positrons data, J. Cosmol. Astropart. Phys. 04 (2014) 006.

[44] S. Recchia, S. Gabici, F. A. Aharonian, and J. Vink, Local fading accelerator and the origin of TeV cosmic ray electrons, Phys. Rev. D **99**, 103022 (2019).

[45] L. O. Drury, Escaping the accelerator: How, when and in what numbers do cosmic rays get out of supernova remnants?, Mon. Not. R. Astron. Soc. **415**, 1807 (2011).

[46] A. R. Bell, K. M. Schure, B. Reville, and G. Giacinti, Cosmic-ray acceleration and escape from supernova remnants, Mon. Not. R. Astron. Soc. **431**, 415 (2013).